Available online at www.sciencedirect.com
ScienceDirect
Trans. Nonferrous Met. Soc. China 34(2024) 1065−1080
Transactions of Nonferrous Metals Society of China
www.tnmsc.cn

Effects of pre-stretch on microstructure, mechanical properties and corrosion resistance of 2A14 aluminum alloy

Lan-ping HUANG[1,2], Long-long HE[1,3], Song LI[1,3], Wen-sheng LIU[1,2], Jing HUANG[1,3], Song-yi CHEN[4,5]

1. Powder Metallurgy Research Institute, Central South University, Changsha 410083, China;
2. State Key Laboratory of Light Weight and High Strength Structural Materials, Central South University, Changsha 410083, China;
3. State Key Laboratory of Powder Metallurgy, Central South University, Changsha 410083, China;
4. Light Alloy Research Institute, Central South University, Changsha 410083, China;
5. Collaborative Innovation Center of Advance Nonferrous Structural Materials and Manufacturing, Central South University, Changsha 410083, China

Received 22 October 2022; accepted 18 December 2023

Abstract: The microstructure, mechanical properties and corrosion behaviors of the peak-aged 2A14 aluminum alloys subjected to pre-stretch prior to artificial aging were investigated. The results indicate that the hardness and strength of the peak-aged alloy can be greatly enhanced via introducing pre-stretch due to the formation of dense and finer θ' precipitates with dispersed distribution in alloy matrix. Pre-stretch prior to peak aging evidently enhances the peak aging hardness and shortens the peak aging time of the alloy. A pre-stretching degree of 7.5% leads to a distinct inhomogeneous distribution of θ' phase, which decreases the ultimate tensile strength. As pre-stretching degree increases, the plasticity, impact toughness and exfoliation corrosion (EXCO) resistance of the peak-aged alloy all gradually decrease, but its resistance to intergranular corrosion (IGC) increases and then decreases.

Key words: 2A14 aluminum alloy; pre-stretch; microstructure; mechanical properties; corrosion resistance

1 Introduction

Age-hardening 2A14 aluminum alloy, as a typical Al−Cu−Mg alloy, owns high specific strength, excellent workability, good heat resistance and weldability, and has been extensively used as structural materials for manufacturing of key components in the aerospace and aircraft fields such as wheel hubs, fuel tank domes, and missile noses [1−6]. Minor Si addition into 2A14 aluminum alloy can obviously accelerate age-hardening response and enhance peak hardness during artificial aging due to heterogeneous nucleation of the strengthening precipitates [7−9]. It is generally known that conventional manufacturing of 2xxx series aluminum alloys often involves a pre-stretching operation before artificial aging, during which the alloy is typically plastically strained no more than 5%, to eliminate the large residual stresses caused by quenching, and to exert a beneficial effect on the precipitation and relevant mechanical properties of the alloy [10−14]. WANG et al [11] have found that the strength and ductility of 2024 aluminum alloy are enhanced when pre-stretching degree is 2%, while other pre-stretching degrees increase the alloy strength but decrease the elongation. ZHANG et al [12] have employed the pre-deformation to 2519 aluminum alloy prior to ageing and discovered that the alloy strength increases while elongation decreases with increasing pre-stretching degree. QUAN et al [13]

Corresponding author: Song LI, Tel: +86-731-88830911, E-mail: ls2011sl@csu.edu.cn
DOI: 10.1016/S1003-6326(23)66454-4

have proposed that pre-straining can promote the peak hardness and reduce the time to reach the peak hardness with the increase of pre-strain for 2524 aluminum alloy. It has also been found that pre-straining can accelerate aging response and increase the peak hardness of Al−4.12Cu−0.66Mg−0.73Si alloy with a medium Cu-to-Mg ratio by promoting the formation of fine θ' precipitates [15]. In addition, the effects of pre-deformation on corrosion properties of 2xxx series aluminum alloys have also been investigated. For example, LIU et al [16] have discovered that the width of the precipitate free zone (PFZ) decreases with increasing pre-deformation degree, resulting in enhancing intergranular corrosion (IGC) resistance of Al−Cu−Mg−Ag alloy by narrowing the passage way of IGC. LI et al [17] have reported that the poor exfoliation resistance is detected in Al−Cu−Mg alloy subjected to pre-straining before natural aging due to the increase in dislocation density. The similar results have also been found in 2024 aluminum alloy under T3 temper [18].

2A14 aluminum alloy parts for the aerospace applications are subjected to alternating load over a long term during the service process, so the demand is relatively high for their comprehensive properties including strength, ductility, toughness, and corrosion resistance. Currently, the effects of pre-deformation before artificial aging on the strength and ductility of 2A14 aluminum alloy have often been investigated, but little work has been focused on its impact toughness and corrosion resistance [19,20]. Therefore, in this work, the effects of various pre-stretching degrees on the precipitation behaviors, microstructure evolution, mechanical properties and corrosion resistances of the aged 2A14 aluminum alloy with high Cu-to-Mg ratio have been investigated. The results provide a reference for the development of Al−Cu−Mg−Si alloys with high performances.

2 Experimental

The nominal and actual chemical compositions of 2A14 aluminum alloy are given in Table 1. The experimental alloy ingots were prepared by conventional casting, as described elsewhere [21]. The as-received ingot was homogenized at 495 °C for 24 h followed by air cooling to room temperature, and then hot extruded at 440 °C with an extrusion ratio of 10:1. Subsequently, the extruded specimens were solution treated at 503 °C for 3 h and then quenched by water to room temperature. After quenching the specimens were pre-stretched along the extrusion direction to various strain levels (0, 1%, 2.5%, 5% and 7.5%) at room temperature at once, and then were immediately aged at 160 °C for different durations to attain the peak hardness. The detailed description for the procedure is shown in Fig. 1.

The hardness values were monitored by Vickers hardness measurements and at least 6 spots for each sample were selected and then the average value was calculated. The mechanical properties of all the samples were carried out by an Instron 3369 testing machine at room temperature with a tensile speed of 2 mm/min. The impact toughness was examined by pendulum impact tests according to ASTM standard E-23-07. The dimensions of the tested specimen were 10 mm × 10 mm × 55 mm and a 45° V-notch with a depth of 2 mm was cut at the center along the length direction. The IGC tests were performed at (35±2) °C for 12 h according to GB/T 7998—2005 standard [22]. The exposed surface was normal to the short transverse (S) direction. The corrosion depth from the cross-sections of samples was measured using optical microscopy (Leica, Wizz, German). The exfoliation corrosion (EXCO) test was carried out according to GB/T 22639—2008 standard. The sample was immersed in the solution (234 g/L NaCl + 50 g/L KNO_3 + 6.5 mL/L HNO_3) at (25±1) °C for 96 h. The corroded surface was photographed and then evaluated according to EXCO ranking standard.

The XRD patterns were detected by X-ray diffractometer (D8 Adwance type) with a step of 2 (°)/min. The diffraction angle was calibrated with Si standard sample and the XRD data were analyzed by Jade software. The microstructural

Table 1 Nominal and actual compositions of 2A14 aluminium alloy (wt.%)

Composition	Cu	Mg	Si	Fe	Mn	Ti	Al
Actual	4.17	0.42	0.70	0.041	0.63	0.023	Bal.
Nominal	3.9−4.8	0.4−0.8	0.6−1.2	0.2	0.4−1.0	0.15	Bal.

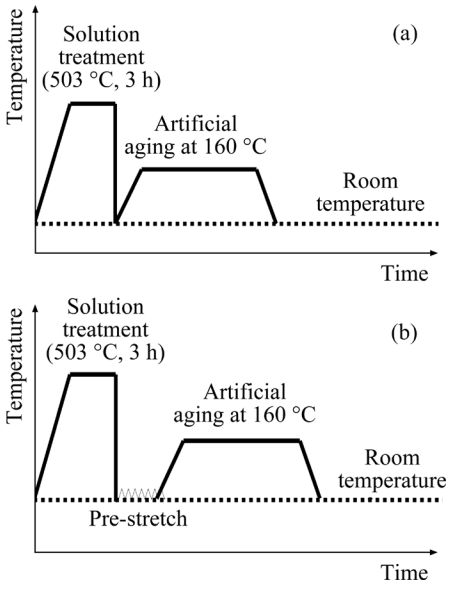

Fig. 1 Schematic diagram of heat treatment process for 2A14 aluminum alloys: (a) Peak aging; (b) Pre-stretch prior to peak aging

observations were performed using optical microscopy (OM, Leica DM4000H, Germany), scanning electron microscopy (SEM, FEI Nova Nano 230) and transmission electron microscopy (TEM, JEM−2100F). Longitudinal−long transverse (L−T) sections of OM specimens were ground, polished and then etched by Keller's reagent. Thin foils for TEM were prepared by mechanical polishing and then twin-jet elector-polishing in 30% HNO_3+70% CH_3OH solution at −20 °C. Differential scanning calorimetry analysis was carried out on a DSC system (DSC 8000) at a rate of 10 K/min.

3 Results

3.1 Microstructure evolution

3.1.1 Optical micrograph

Figure 2 shows the optical micrographs of L−T sections of the peak-aged 2A14 aluminum alloys subjected to various pre-stretching degrees. It can be seen that the alloy grains are elongated along the extrusion direction, and coarse crystalline phases are distributed in chain-like conformation along grain boundaries. With the increase of pre-stretching degree, the elongated grains become longer and narrower along the extrusion direction. As shown in Figs. 2(c−e), the aspect ratio of alloy grains increases significantly when pre-stretching degree is no less than 2.5%.

3.1.2 DSC analysis results

Figure 3 shows the DSC curves of 2A14 aluminum alloys after solution treatment and the peak-aged ones subjected to various pre-stretching degrees. It can be seen that all the samples have two exothermic peaks (labeled as A and C) and two endothermic peaks (labeled as B and D) in the temperature range between 200 and 350 °C. These four peaks correspond to the precipitation of Q' and θ' phases (A and C) and the dissolution of Q' and θ' phases (B and D), respectively, as described elsewhere [6,23]. The precipitation peak temperatures of Q' and θ' phases in the peak-aged 2A14 aluminum alloy subjected to various pre-stretching degrees are given in Table 2. With the increase of pre-stretching degree, the precipitation peak

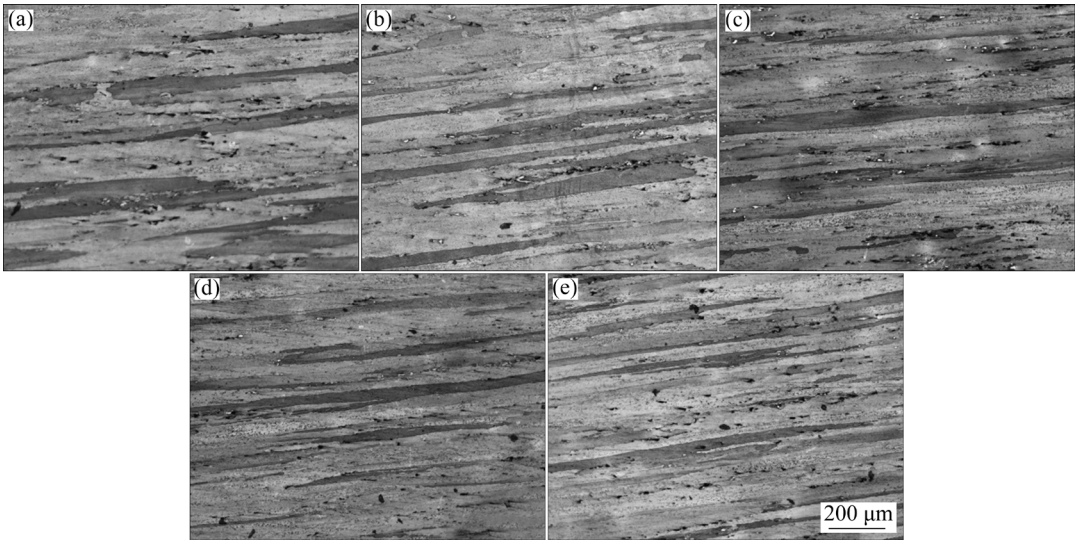

Fig. 2 Optical micrographs for L-T sections of peak-aged 2A14 aluminum alloys subjected to various pre-stretching degrees: (a) 0; (b) 1%; (c) 2.5%; (d) 5%; (e) 7.5%

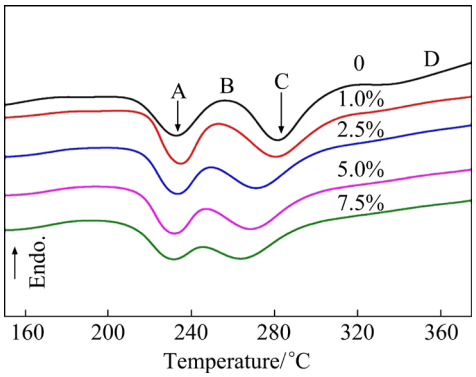

Fig. 3 DSC curves of 2A14 aluminum alloys after solution treatment and peak-aged ones subjected to various pre-stretching degrees at heating rate of 10 K/min

Table 2 Precipitation peak temperatures of Q' and θ' phases of samples with various pre-stretching degrees

Pre-stretching degree/%	Peak temperature of Q' phase/°C	Peak temperature of θ' phase/°C
0	232.51	281.64
1	234.85	280.01
2.5	233.23	270.95
5	233.46	267.72
7.5	231.86	263.32

temperature of Q' phase does not change much, and is (233±2) °C. However, the precipitation peak temperature of θ' phase varies greatly with pre-stretching degree. Compared with the alloy without pre-stretch, the peak corresponding to the precipitation of θ' phase slightly shifts to the left (less than 2 °C). When the pre-stretching degree increases from 1% to 2.5%, the precipitation peak of θ' phase shifts to the left by about 10 °C. With the further increase of pre-stretching degree, the precipitation peak temperature of θ' phase also continues to decrease. This may be due to the dislocations introduced by pre-stretch which accelerate the diffusion of solute atoms in solid solution and promote the nucleation of precipitated phase.

3.1.3 XRD data for dislocation density

In order to estimate the effect of pre-stretching degree on dislocation density of the studied alloys, the XRD data have been obtained and analyzed by Jade software. Figure 4(a) presents the XRD patterns of the peak-aged 2A14 aluminum alloys subjected to various pre-stretching degrees. It can be confirmed that the studied alloys mainly consist

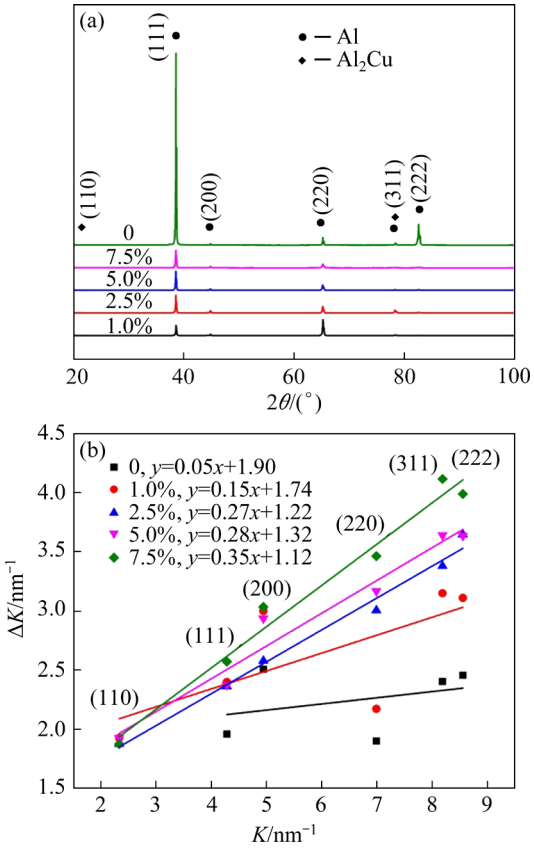

Fig. 4 XRD analysis results of peak-aged 2A14 aluminum alloys subjected to various pre-stretching degrees: (a) Diffraction pattern; (b) Curves of ΔK−K

of A1 matrix and $A1_2Cu$ (θ) phase. Though the 2A14 aluminum alloys subjected to various pre-stretching degrees indicate very similar diffraction patterns, there are still a few differences in these alloys. Dislocation density can be estimated based on XRD data by the modified Williamson−Hall method [24,25]. According to the equations described in Ref. [24], dislocation density is believed to be approximately proportional to the slope of ΔK−K curves. $K=2\sin\theta/\lambda$ and $\Delta K=2\Delta\theta\cos\theta/\lambda$, where θ is the diffraction angle, λ is the wavelength of the X-rays, and $\Delta\theta$ is the full width of half maximum (HFWH) for diffraction peak. Figure 4(b) presents the relationship between ΔK and K for the peak-aged 2A14 aluminum alloys subjected to various pre-stretching degrees based on the modified Williamson−Hall method. According to the fitted slopes of ΔK−K curves in Fig. 4(b), the pre-stretch prior to artificial aging distinctly enhances the dislocation density of 2A14 aluminum alloy and its dislocation density increases with pre-stretching degree.

3.1.4 TEM microstructure

In order to further understand the effect of dislocations on the aging precipitates of 2A14 aluminum alloy, TEM experiment has been carried out. Figure 5 shows the TEM bright-field images and the corresponding selected area electron diffraction (SEAD) patterns along the $[001]_{Al}$ zone axes of the peak-aged 2A14 aluminum alloys subjected to various pre-stretching degrees as well as the schematic diagrams of diffraction patterns of θ' and Q' phases [26,27]. The TEM image and corresponding SEAD pattern of the peak-aged alloy without pre-stretch in Figs. 5(a, b) present that there are mainly two kinds of the precipitates evenly distributed in the matrix, fine-dots and lath-like phases. As shown in Figs. 5(b, g, h), the corresponding diffraction fringes are the characteristic diffraction fringes of Q' and θ' phases. The faint streaks corresponding to θ' phase are found at the position of $(110)_{Al}$ along the $[010]_{Al}$ and $[100]_{Al}$ directions, while the diffraction spots corresponding to Q' phase occur at the position of $(020)_{Al}$ along the [001]

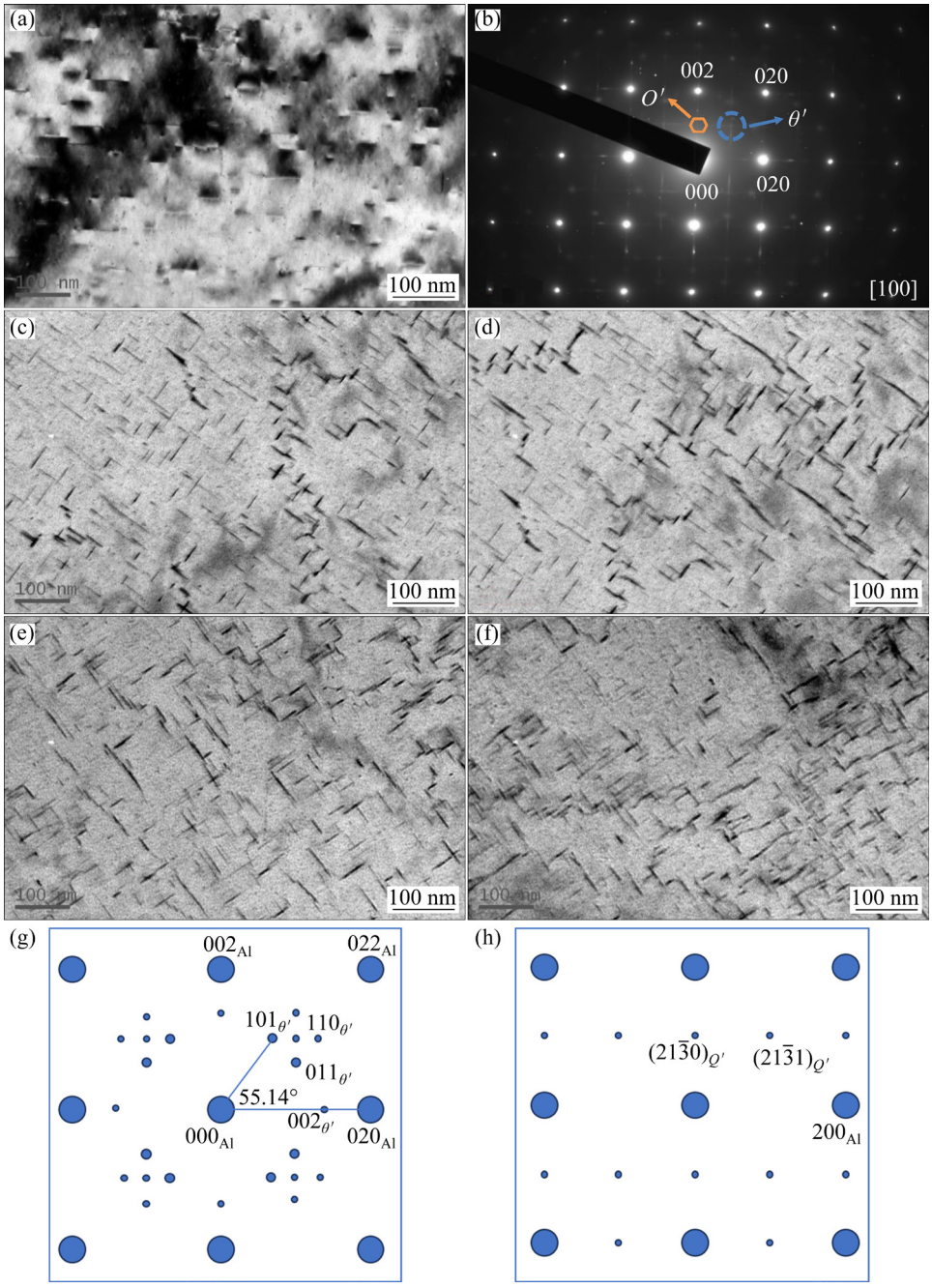

Fig. 5 TEM bright-field images and corresponding SEAD patterns along $[001]_{Al}$ zone axes of peak-aged 2A14 alloys subjected to various pre-stretching degrees ((a, b) 0; (c) 1%; (d) 2.5%; (e) 5%; (f) 7.5%) and schematic diagrams of diffraction patterns of θ' phase (g) and Q' phase (h)

zone axis. The hardness and strength of the alloy mainly depend on the strengthening effect of the uniformly distributed θ' and Q' phases. When pre-stretching degree is 1%, it can be found from Fig. 5(c) that the number of θ' phases in the alloy matrix increases compared with the alloy without pre-stretch. After further increasing the pre-stretching degree from 1% to 2.5%, the number of θ' phases also further increases and its distribution is relatively uneven, but the average dimension of θ' phases is slightly larger than that of the sample with 1% pre-stretching degree (Fig. 5(d)). As shown in Fig. 5(e), the distribution of θ' phases in the peak-aged alloy with 5% pre-stretching degree is heterogeneous and its size is also different. The coarsening of a portion of θ' phases is obvious. When the pre-stretching degree is 7.5%, the distribution of θ' phases is more uneven in the alloy matrix (Fig. 5(f)). The distribution density of θ' phases is relatively higher in some regions shown in the upper-right area of Fig. 5(f) and fairly sparse in some regions (upper-middle area in Fig. 5(f)). Compared with θ' phase, the number and size of Q' phases do not change much with increasing pre-stretching degree. The pre-stretch prior to artificial aging has a great influence on the precipitation of θ' phase in 2A14 aluminum alloy. This suggests that θ' phase is more sensitive to the dislocations than Q' phase, which is consistent with the above DSC results (Fig. 3).

Figure 6 shows the TEM images focusing on the grain boundary of the peak-aged 2A14 aluminum alloys subjected to various pre-stretching degrees. As pre-stretching degree increases from 0 to 7.5%, the distribution of the precipitates on grain boundaries gradually changes from a continuous chain to discontinuity and the size of the precipitates decreases significantly. Compared with the alloys with pre-stretch (Figs. 6(b−e)), the precipitation free zone (PFZ) of the alloy without

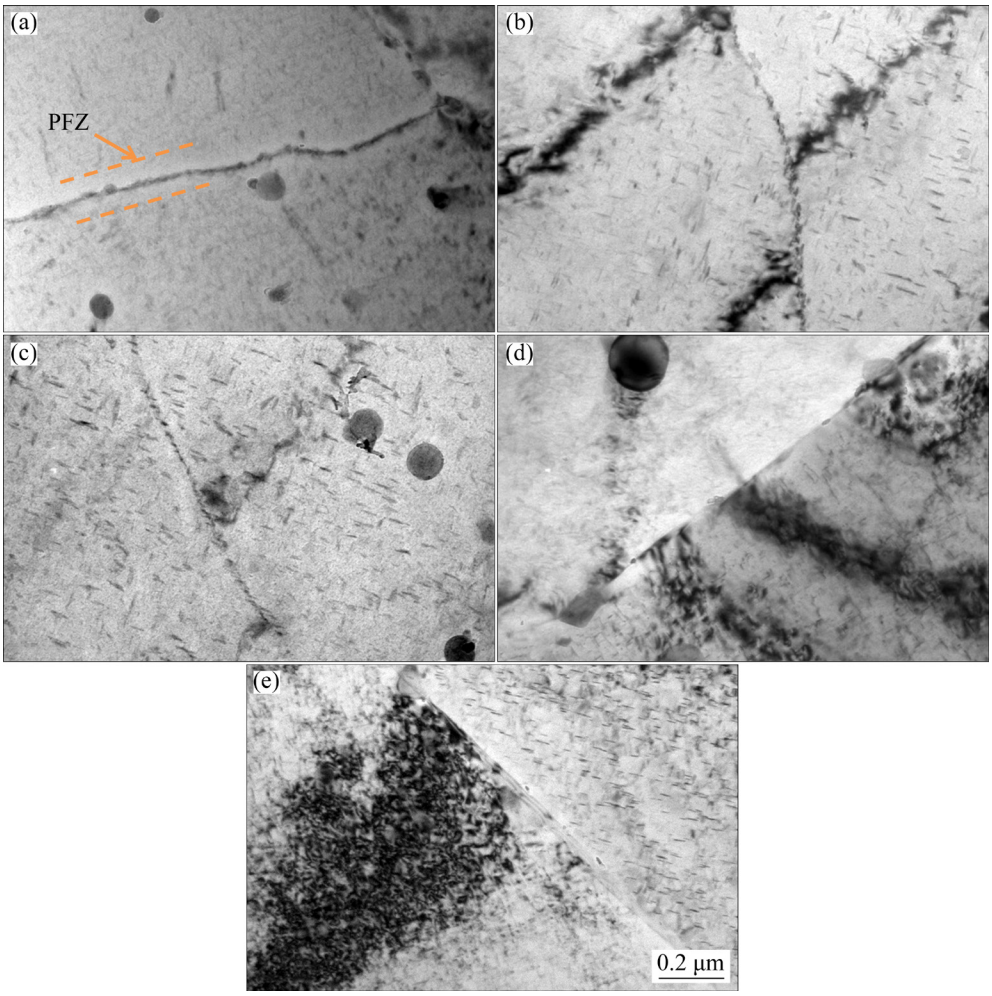

Fig. 6 TEM images focusing on grain boundaries of peak-aged 2A14 aluminum alloys subjected to various pre-stretching degrees: (a) 0; (b) 1%; (c) 2.5%; (d) 5%; (e) 7.5%

pre-stretch is more obvious (Fig. 6(a)). With the increase of pre-stretching degree, the width of PFZ decreases. It is worth noting that the dislocations also occur on grain boundaries when pre-stretching degree is 7.5%.

3.2 Mechanical properties

3.2.1 Age hardening curves

The age hardening curves of 2A14 aluminum alloys with various pre-stretching degrees ranging from 0 to 7.5% aged at 160 °C for up to 30 h are shown in Fig. 7(a). It can be found that the initial hardness value of 2A14 aluminum alloy increases as pre-stretch degree increases up to 7.5%. The initial hardness of the as-quenched alloy is about HV 105, while the highest initial hardness value of HV 139 can be attained for the alloy with a pre-stretching degree of 7.5%. Working hardening is responsible for the increase of the initial hardness with the increase of the pre-stretching degree. Otherwise, all the hardness variations of the alloys subjected to various pre-stretching degrees on aging time exhibit a similar trend. At the initial stage of aging, the hardness rapidly increases, and then attains the peak value. To further clarify the peak hardness and aging time, the partial enlarged drawings of aging hardening curves of the alloys are shown in Fig. 7(b). It can be seen that the peak hardness is HV 158 at 16 h for the alloy without pre-stretch. After applying pre-stretching degrees of 1%, 2.5%, 5% and 7.5%, the peak hardness is about HV 160, HV 162, HV 164 and HV 162, respectively, while the time required for achieving the peak hardness is about 14, 14, 12 and 12 h, respectively. The increase of pre-stretching degree prior to artificial aging enhances the peak hardness of the alloy and reduces the time to reach peak hardness.

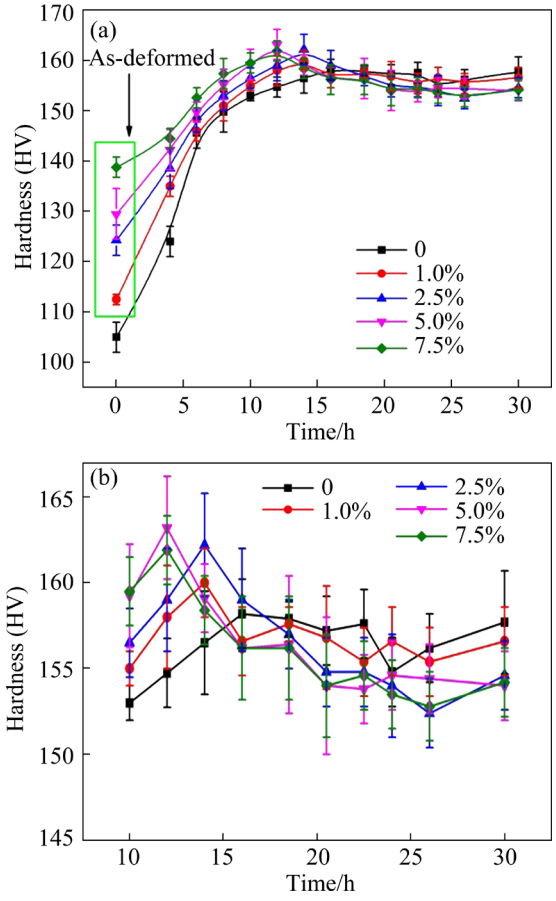

Fig. 7 Aging hardening curves of 2A14 aluminum alloys subjected to various pre-stretching degrees at 160 °C for 30 h (a); Hardness variations on aging time after 10 h (b)

3.2.2 Tensile properties

The tensile properties of the peak-aged 2A14 aluminum alloys subjected to various pre-stretching degrees are summarized in Fig. 8 and Table 3. As shown in Fig. 8(a), the ultimate tensile strength (UTS) increases with the increase of pre-stretching degree before reaching a maximum value of 538 MPa at a pre-stretching degree of 5%, but slight decreases to 525 MPa when pre-stretching degree further increases to 7.5%. The yield strength (YS) increases continuously as the pre-stretching degree increases from 0 to 7.5% (Fig. 8(b)). However, it is also clearly seen from Fig. 8(c) that the elongation decreases continuously with the increase of pre-stretching degree. The maximum value of YS is 502 MPa at a pre-stretching degree of 7.5%, while the maximum value of elongation is about 10.5% for the alloy without pre-stretch. The results show that pre-stretch prior to artificial aging can effectively improve the strength of the peak-aged 2A14 aluminum alloy, but reduce its plasticity.

3.2.3 Tensile fracture morphology

Figure 9 shows the SEM images of tensile fracture morphologies of the peak-aged 2A14 aluminum alloys subjected to various pre-stretching degrees. For the alloy without pre-stretch, as shown in Fig. 9(a_1), the fracture surface is composed of tearing edges and dimples with various sizes, indicating a mixed model of dimple-induced trans-granular fracture and intergranular fracture. Figure 9(a_2) presents the enlarged view of the green box in Fig. 9(a_1). It can be found that most of dimples are small, but there are some large dimples with a size of about 9 μm. Besides, there are some

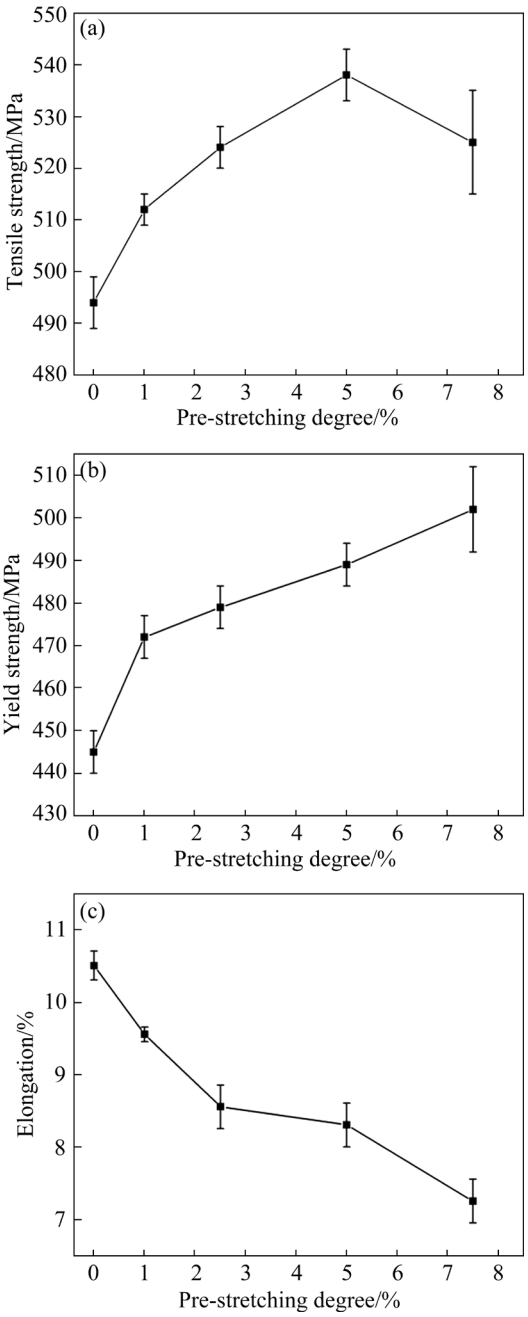

Fig. 8 Room-temperature tensile properties of peak-aged 2A14 aluminum alloys subjected to various pre-stretching degrees: (a) Tensile strength; (b) Yield strength; (c) Elongation

second-phase particles inside dimples and small dimples are distributed around the large dimples. As pre-stretching degree increases from 1% to 7.5%, it can be seen from Figs. 9(b_1−d_1) that the size of the dimple becomes smaller and its depth gets shallower. Otherwise, the area dominated by the flat plane on the fracture also gradually increases. A significant intergranular brittle fracture characteristic is found on the fracture of the alloy

Table 3 Mechanical properties of peak-aged 2A14 aluminum alloys subjected to various pre-stretching degrees

Pre-stretching degree/%	Ultimate tensile strength/MPa	Yield strength/MPa	Elongation/ %
0	494	445	10.51
1.0	512	472	9.56
2.5	524	479	8.56
5.0	538	489	8.31
7.5	525	502	7.26

with a pre-stretching degree of 7.5%, which indicates that the increase of pre-stretching degree is detrimental to the plasticity of the peak-aged 2A14 aluminum alloy. This fracture behavior is consistent with the curve shown in Fig. 8(c).

3.2.4 Impact toughness and impact fracture surfaces

Figure 10 presents the relationship between the absorbed energies of the peak-aged 2A14 aluminum alloys subjected to various pre-stretching degrees during impact testing and pre-stretching degrees. The impact toughness represents the ratio of absorbed impact energy to area of fracture. As shown in Fig. 10, the absorbed energy of the alloy without pre-stretch is 12.98 J/cm^2. With the increase of pre-stretching degree, the absorbed impact energy gradually decreases. At a pre-stretching degree of 7.5%, the lowest absorbed energy of 9.55 J/cm^2 is attained. This suggests that the increase of pre-stretching degree results in the decrease of impact toughness for the peak-aged 2A14 aluminum alloys.

Figure 11 shows the SEM images of impact fracture morphologies of the peak-aged 2A14 aluminum alloys with pre-stretching degrees of 0, 2.5% and 7.5%. As shown in Figs. 11(a, b, c), the crack initiation zones of all the samples are relatively flat and close to the V-notch root, which essentially exhibits the initial fracture under impact loading after local shear deformation along the maximum shear stress direction [28]. The width of crack initiation zone (W_{ci}) has been measured by Image J software. The W_{ci} value of alloy without pre-stretch is 81 μm and higher than that of the ones with pre-stretching degrees of 2.5% (52 μm) and 7.5% (39 μm), which suggests the decreased energy consumption for crack initiation under the larger pre-stretching degree. According to the previous reports [28], the crack initiation energy dominates

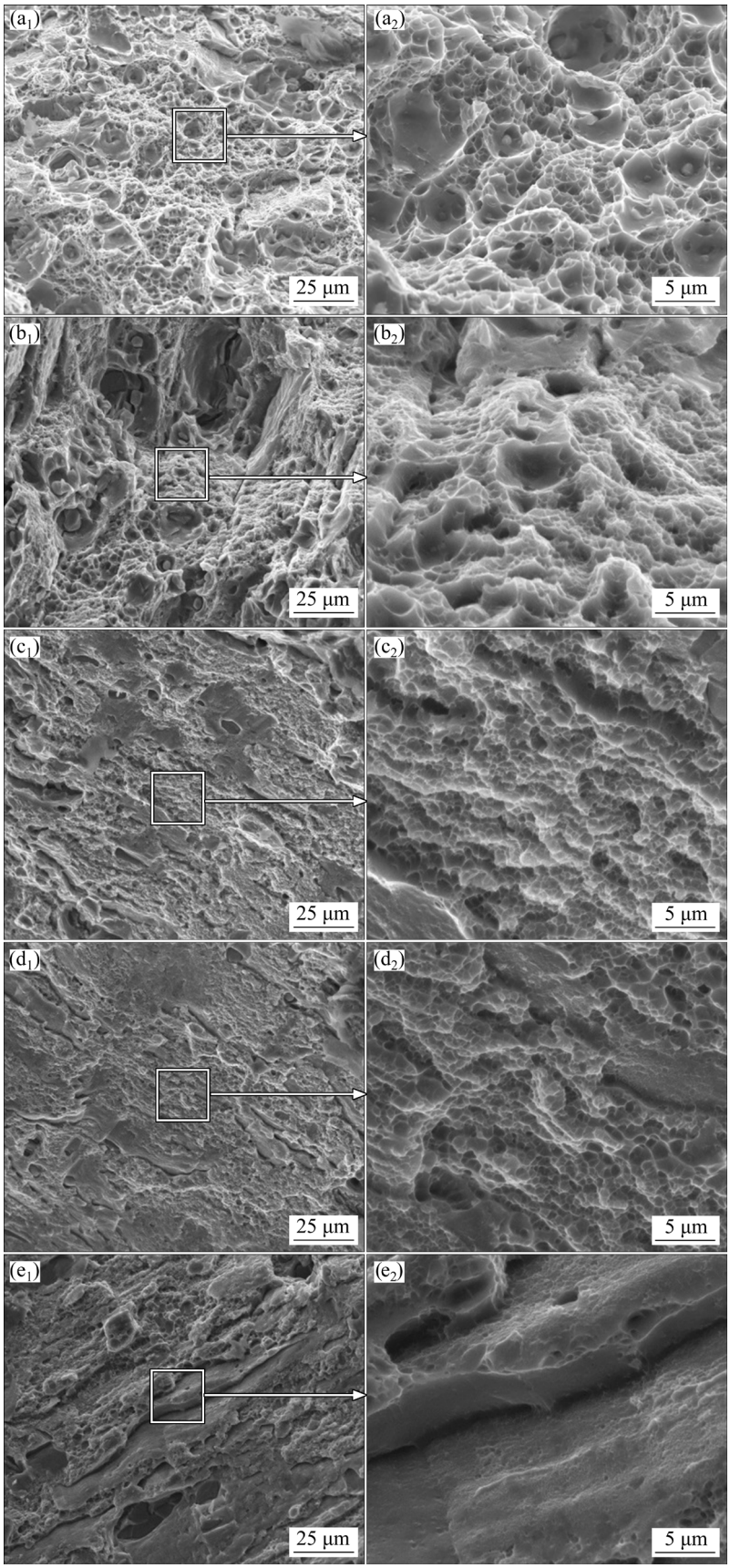

Fig. 9 SEM images of tensile fracture morphologies of peak-aged 2A14 aluminum alloys subjected to various pre-stretching degrees: (a_1, a_2) 0; (b_1, b_2) 1%; (c_1, c_2) 2.5%; (d_1, d_2) 5%; (e_1, e_2) 7.5%

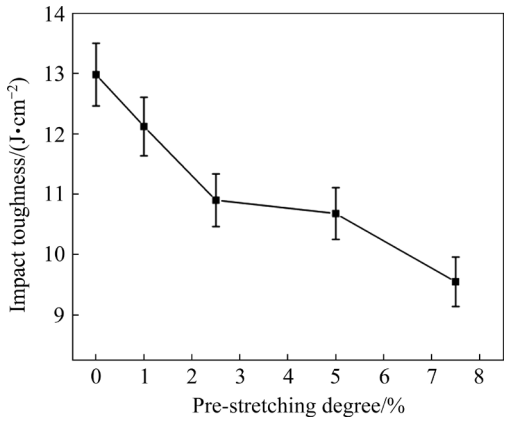

Fig. 10 Impact toughness of peak-aged 2A14 aluminum alloys subjected to various pre-stretching degrees

the total fracture energy of the alloy under impact loading, so the impact toughness of 2A14 aluminum alloy decreases with the decrease of W_{ci} induced by increasing pre-stretching degree. In the high-magnification view (shown in Figs. 11(d, e, f)), a typical ductile fracture characteristic consisting of densely distributed small dimples and relative larger ones (with diameter more than 10 μm) occurs on fracture surface for all the samples. With the increase of pre-stretching degree, much shallower and relatively larger dimples increase on fracture surface, which consumes much lower fracture energy, leading to the decrease of impact toughness for the peak-aged 2A14 aluminum alloy. Moreover, some micro-cracks occur in the root of relatively large dimples when pre-stretching degree is up to 7.5%.

3.3 Corrosion properties

3.3.1 IGC resistance

The cross-section corrosion morphologies and maximum corrosion depths of the peak-aged 2A14 aluminum alloys subjected to various pre-stretching degrees are shown in Figs. 12 and 13, respectively. Maximum corrosion depth is used to evaluate IGC resistance of the alloy. As shown in Figs. 12 and 13, the corrosion extends along grain boundaries and the depth of corrosion attack changes with pre-stretching degrees. The alloy without pre-stretch exhibits severe IGC susceptibility and its corrosion area and depth both are the largest for all the samples. The IGC depth for the alloy without pre-stretch is found to be about 290 μm. As pre-stretching degree increases from 0 to 5.0%, the IGC depth of the alloy gradually decreases. When pre-stretching degree is up to 5.0%, the IGC depth reaches the minimum value (about 193 μm). Further increasing pre-stretching degree to 7.5%, the IGC depth of the alloy is about 225 μm, which is deeper than that of the alloy with a pre-stretching degree of 5.0%.

3.3.2 Exfoliation corrosion (EXCO) resistance

The visual EXCO ratings of the peak-aged 2A14 aluminum alloys subjected to various pre-stretching degrees after immersion for various time are listed in Table 4. It can be found that the degree of corrosion increases to various levels with the extension of immersion time for all the samples. The corrosion rate of N (No appreciable attack) is given for all the samples after immersion for 6 h due to no pitting or exfoliation corrosion on surface. Increasing pre-stretching degree can obviously increase the EXCO susceptibility. When the immersion time is no more than 48 h, no severe pitting, blistering or delamination is seen for the peak-aged 2A14 aluminum alloys with the pre-stretching degrees of 0, 1%, 2.5%, and 5%, but

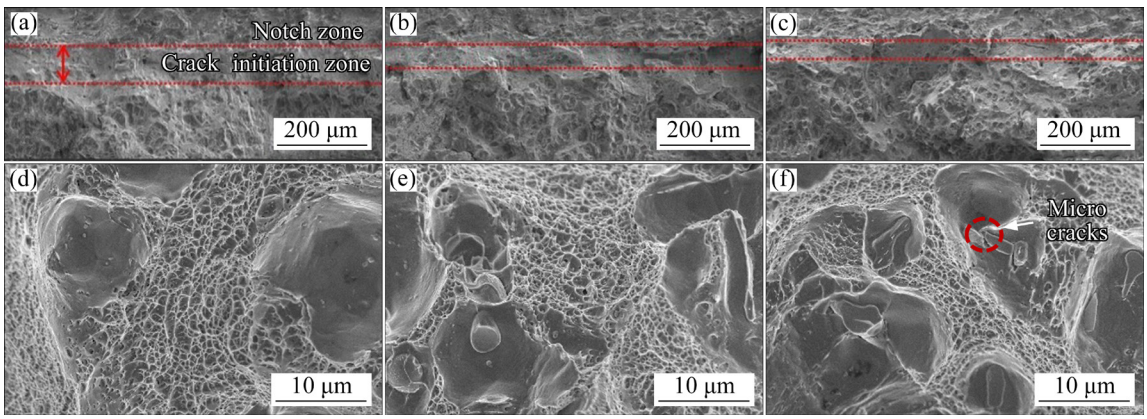

Fig. 11 SEM images of impact fracture morphologies of peak-aged 2A14 aluminum alloys subjected to various pre-stretching degrees: (a, d) 0; (b, e) 2.5%; (c, f) 7.5%

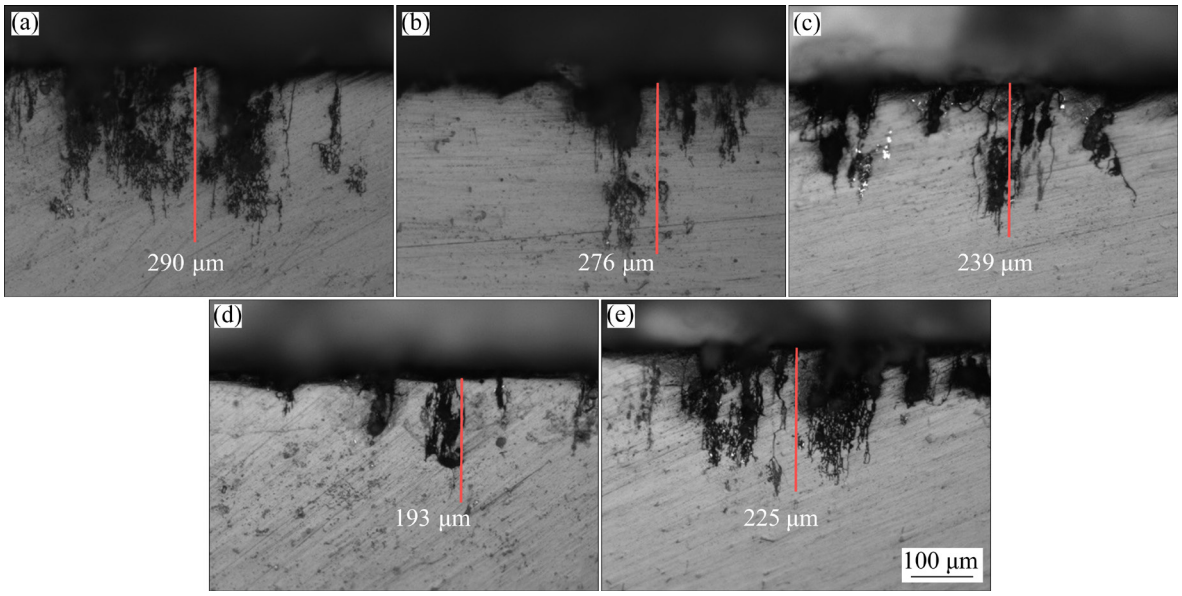

Fig. 12 SEM images of cross-section corrosion morphologies of peak-aged 2A14 aluminum alloys subjected to various pre-stretch degrees: (a) 0; (b) 1%; (c) 2.5%; (d) 5%; (e) 7.5%

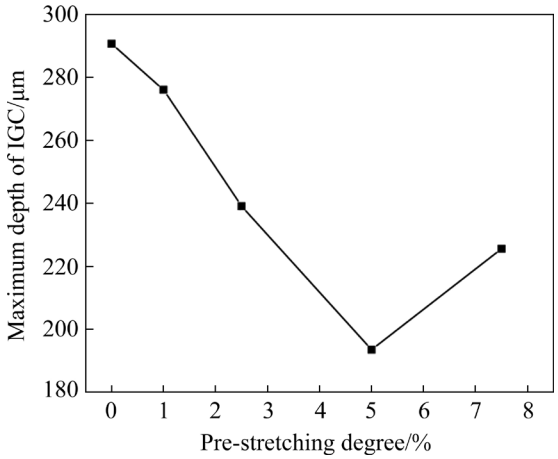

Fig. 13 Maximum corrosion depths of peak-aged 2A14 aluminum alloys subjected to various pre-stretch degrees

Table 4 Exfoliation corrosion levels of peak-aged 2A14 aluminum alloys with various pre-stretching degrees after different immersing time

Pre-stretching degree/%	Immersion time/h				
	6	24	48	72	96
0	N	PA	PC	PC	EA
1.0	N	PA	PA	PC	EA
2.5	N	PA	PB	PC	EB
5.0	N	PB	PC	EA	EC
7.5	N	PB	EA	EB	ED

N−No appreciable attack; PA−Slight pitting; PC−Severe pitting; EA−Superficial exfoliation; EB−Severe exfoliation; EC−Severe exfoliation and penetration; ED−Very severe exfoliation

blisters with several millimeters in diameter and delamination occur on the surface of the sample with a pre-stretching degree of 7.5% and its EXCO rate is ranked as EA (superficial exfoliation). After immersed for 72 h, the EXCO rates are ranked as EA and EB when pre-stretching degree is no less than 5%, respectively. Figure 14 shows the EXCO macrographs of the peak-aged 2A14 aluminum alloys subjected to various pre-stretching degrees after immersion for 96 h. As shown in Figs. 14(a, b), only superficial exfoliation (EA) can be found on the surfaces of the samples without pre-stretch and with a pre-stretching degree of 1%, indicating that they have good EXCO resistances. When further increasing pre-stretching degree from 2.5% to 7.5%, it can be seen from Figs. 14(c−e) that notable delamination and penetration occur on the surfaces of the samples and their EXCO rates increase from EB (severe exfoliation) to ED (very severe exfoliation). The above results show that the EXCO resistance of the peak-aged 2A14 aluminum alloy decreases with increasing pre-stretching degree.

4 Discussion

4.1 Effects of pre-stretch on precipitation behaviors during aging

As a Al−Cu−Mg−Si alloy with high Cu-to-Mg ratio, the precipitation processes of 2A14 aluminum alloy can be summarized as follows [23,29,30]:

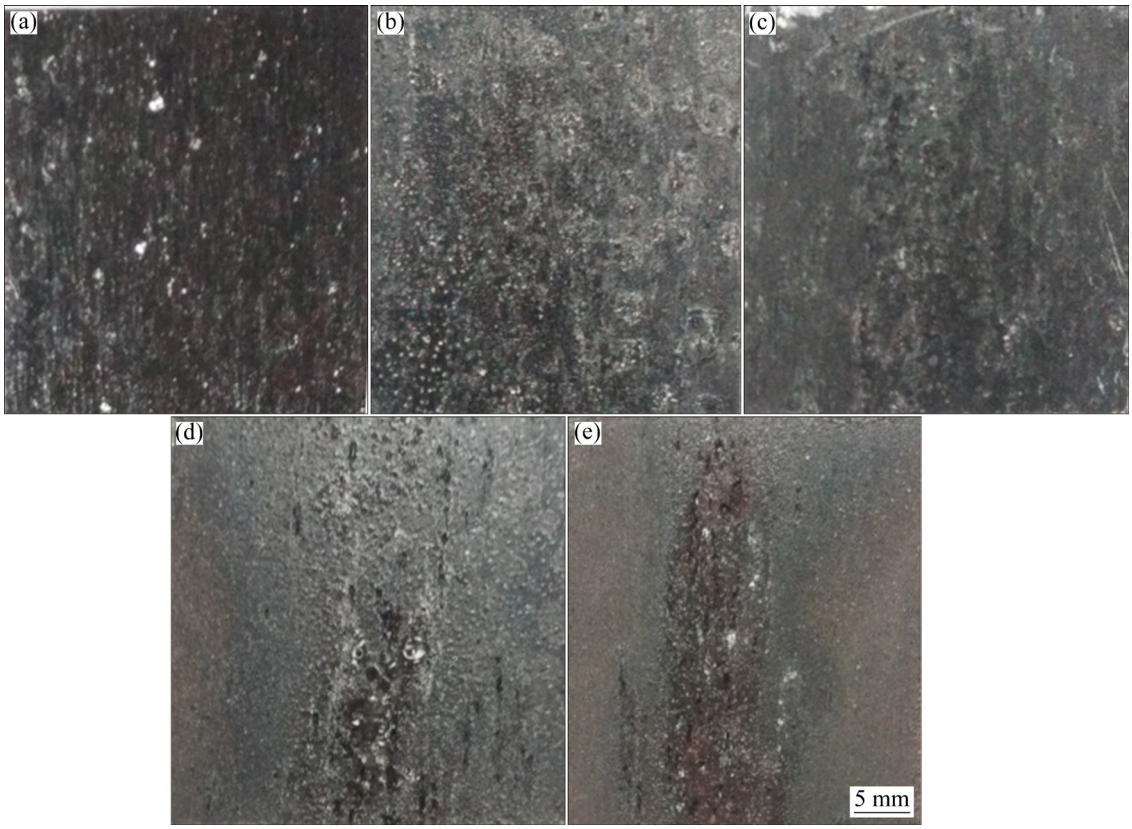

Fig. 14 EXCO macrographs of peak-aged 2A14 aluminum alloys subjected to various pre-stretching degrees after immersion for 96 h: (a) 0; (b) 1%; (c) 2.5%; (d) 5%; (e) 7.5%

(1) Supersaturated solid solution (SSS) → Clusters → Guinier−Preston (GP) zones→ θ''→ θ' → θ (Al_2Cu); (2) SSS → Guinier−Preston−Bagaryatsky (GPB) zones → S'' → S' → S (Al_2CuMg); (3) SSS → GP zones → Q' → Q ($Al_5Cu_2Mg_8Si_6$, $Al_3Cu_2Mg_9Si_7$ or $Al_4Cu_2Mg_8Si_7$). The precipitation sequence during artificial aging depends mainly on Cu-to-Mg and Mg-to-Si ratios in Al−Cu−Mg−Si alloy system. It has been shown that, when the Cu-to-Mg ratio is in the range of 4%−8% and Cu content is more than 1.0 wt.%, the main strengthening phases are θ' and S' with coherent or semi-coherent configuration in Al−Cu−Mg alloys. The introduction of Si can change the aging precipitation sequence of Al−Cu−Mg alloys. The secondary strengthening phases in Al−Cu−Mg−Si alloys are θ', S' and β' phase if the ratio of Mg-to-Si is more than 2:1. However, the precipitation behavior of Al−Cu−Mg−Si alloys with a ratio of Mg-to-Si lower than 1:1 is more complicated, and the Q', θ', and S' phases as well as their precursors can be found [20,27,31,32]. From Fig. 5, it can be seen that the θ' and Q' phases coexist in the peak-aged 2A14 aluminum alloys with and without pre-stretch, and no S' phase is observed. The presence of Si contributes to the formation of Mg-containing dot-like Q' precipitates owing to the strong binding energy between Si and Mg at the early stage of aging [33]. Besides, RINGER et al [34] also have found that it is easier for Cu−Cu cluster to form GP zones rather than GPB zones in Al−Cu−Mg−Si alloys with Mg content below 0.8 wt.%. Therefore, the formation of S' phase is suppressed in the investigated alloys.

As shown in Figs. 5(d, e), the number of fine θ' precipitates extremely increases as pre-stretching degree increases to 2.5%, while the distribution of θ' precipitates is relatively uneven and its size is also obviously different when pre-stretching degree is up to 5%. After the as-quenched alloys are subjected to pre-stretch prior to artificial aging, a large number of dislocations are introduced in the alloy matrix. The dislocations can provide the channels for short-range diffusion [16,35], leading to the decrease of activation energy for diffusion and the acceleration of solute atomic diffusion. This can facilitate the θ' nucleation and increase its distribution density. Otherwise, the relatively higher

energy at the dislocations in alloy matrix offers the required strain energy for the nucleation of strengthening phase [12,16,35]. This also reduces the energy required for the nucleation of θ' phase, resulting in the decrease of its precipitation temperature (Fig. 3). The θ' distribution becomes more uneven when further increasing pre-stretching degree to 7.5%. This non-uniform distribution is closely linked with the formation of dislocation cells, which more easily occur for the alloy with higher pre-stretching degree. When pre-stretch increases to a certain degree, excessive dislocations occur in alloy matrix and some of them entangle with each other, leading to the formation of dislocation cells. The dislocation density within the cells is distinctly higher than that on the cell walls, which results in the non-uniform θ' distribution within the cells and on the cell walls.

As pre-stretching degree increases from 0 to 7.5%, the distribution of the grain-boundary precipitates gradually changes from continuous to discontinuous and their size decreases significantly (Fig. 6). A large number of dislocations occur in grain interiors due to pre-stretch and then can act as preferential positions for the nucleation of precipitates. The distinct increase of the precipitates in grain interiors makes solute atoms in alloy matrix decrease, which leads to the discontinuous distribution of the grain-boundary precipitates. Meanwhile, the resistance to dislocation movement is relatively low during pre-stretch prior to artificial aging, so most of dislocations are easy to be blocked near grain boundaries and induce the formation of dislocation pile-ups near grain boundaries. During subsequent aging, the increase of dislocation density near grain boundaries induced by dislocation pile-ups prompts the diffusion of solute atoms near grain boundaries. This makes the PFZ formation very difficult, so its width becomes narrower with the increase of pre-stretching degree. However, for the alloy without pre-stretch, solute atoms near grain boundaries are mainly consumed to form the grain-boundary precipitates, resulting in a wider PFZ.

4.2 Effects of pre-stretch on mechanical properties

It is well known that θ' phase is the main strengthening phase rather than Q' phase in 2A14 aluminum alloys according to Refs. [31,36,37]. Otherwise, as shown in Fig. 5, the number and size of Q' phases do not change much with the increase of pre-stretching degree. Therefore, the increase in peak strength of the peak-aged 2A14 aluminum alloy with increasing pre-stretching degree is closely linked with the distribution, number density and size of θ' phases. When pre-stretching degree increases to 2.5%, the number of θ' phases obviously increases and its size becomes slightly larger (Figs. 5(a−d)). The relatively larger distribution density of θ' phases in alloy matrix is responsible for the increase of peak strength of the alloy with pre-stretch. Besides, the dislocations introduced by pre-stretch prior to artificial aging can offer the channels for the diffusion of solute atoms, which helps to enhance the growth rate of aging precipitates, so the time to reach peak hardness decreases for the alloy with pre-stretch. When pre-stretching degree further increases up to 7.5%, the yield strength of the alloy also continuously increases but its tensile strength slightly decreases than that of the alloy with a pre-stretching degree of 5%. This suggests that the improvement in the strengthening effect of aging precipitates is limited by increasing pre-stretching degree. Otherwise, as shown in Fig. 5(f), the distribution of the precipitates is uneven, which is unfavorable for the enhancement of tensile strength and ductility of the alloys [12].

In the peak-aged 2A14 aluminum alloys, the number of precipitates in grain interiors increases and the spacing among precipitates decreases as pre-stretching degree increases, which leads to the incompatibility between the relatively hard precipitates and Al alloy matrix during deformation. This incompatibility causes these second-phase precipitates to detach from Al matrix around them and then results in the formation of micro-cracks under severe deformation. These micro-cracks are interconnected and ultimately cause the fracture of 2A14 aluminum alloy [21]. Therefore, the elongation and impact toughness of the peak-aged 2A14 aluminum alloy decrease as pre-stretching degree increases. Otherwise, it can be found from Fig. 6(e) that there are still dislocation pile-ups in the peak-aged alloy subjected to the relatively high pre-stretching degree, which makes dislocation glide inhibited during deformation. This also results in the loss of ductility and toughness.

4.3 Effects of pre-stretch on corrosion properties

During the service process of aluminum alloys, IGC, as a common form of local corrosion, can destroy the bonding force among grains, resulting in a significant decrease in mechanical properties of aluminum alloys. The IGC is considered to be developed from electrochemical corrosion, so the difference of electrochemical heterogeneity plays a dominate role in IGC of aluminum alloys between grain boundary and its surrounding microstructure, including the width of PFZ, and the potential difference between PFZ and the matrix as well as the size and distribution of grain-boundary precipitates. It is well accepted that Cu content in PFZ is lower than that of alloy matrix or grain-boundary precipitates (GBPs) [38,39]. Therefore, the self-corrosion potential of PFZ is more negative than that of Al alloy matrix and GBPs, which acts as the anode during corrosion. As shown in Figs. 12 and 13, with the increase of pre-stretching degree, the width of PFZ decreases, so the IGC resistance of the alloy is obviously enhanced because the wider PFZ is more easily subjected to preferential dissolution and Al matrix is still stable during IGC. Otherwise, compared with the continuously distributed GBPs in the alloy without pre-stretch, the discontinuous distribution of grain-boundary precipitates is unfavorable for the development of IGC (Fig. 6). It is worth noting that the IGC resistance of the alloy slightly decreases when the pre-stretching degree increases from 5% to 7.5%. This may be linked with the existence of dislocations on grain boundaries. The dislocations pinned on grain boundaries can make strain energy near grain boundaries increase, which promotes IGC more likely to occur [18,40].

As a particular form of IGC, EXCO is often observed on the surface of aluminum alloys with an elongated grain structure [41]. As shown in Fig. 14, EXCO generally proceeds along intergranular paths parallel to the surface. During immersion, the volume of corrosion products formed is larger than that of the initial alloy matrix from which the product is formed, which results in a wedging stress that may lift up the surface grains and induce a layered appearance. It is well known that the susceptibility of EXCO is closely linked with the grain aspect ratio of the alloy [42,43]. The alloy with grains of higher aspect ratio shows higher EXCO susceptibility. It can be seen from Fig. 2 that the grain aspect ratio of the alloy increases distinctly when pre-stretching degree is no less than 2.5%. Therefore, the EXCO susceptibility of the alloy gradually decreases with the increase of pre-stretching degree.

5 Conclusions

(1) Pre-stretch prior to artificial aging enhances the aging kinetics of the alloy, reflected by the lower precipitation temperature of θ' phase, faster aging hardening behavior and higher peak hardness, and facilitates the θ' phase formation. With the increase of pre-stretching degree, the tensile strength and yield strength of the alloy both increase but the ductility and impact toughness gradually decrease. The number density of θ' phase increases as pre-stretching degree increases, but an over high pre-stretching degree (7.5%) results in a distinct inhomogeneous distribution of θ' phase, which makes the ultimate tensile strength slightly lower compared with that at a pre-stretching degree of 5%.

(2) As pre-stretching degree increases, the continuous distribution of the grain-boundary precipitates becomes evidently discontinuous and the PFZ width is narrower, which leads to the enhancement of IGC resistance of the alloy. However, when pre-stretching degree is up to 7.5%, the IGC resistance slightly decreases due to the increase of strain energy on grain boundaries induced by the over high pre-stretching degree. Otherwise, the increase of pre-stretching degree results in the increased susceptibility to EXCO of the alloy because of the higher grain aspect ratio. The distribution of grain-boundary precipitates, the PFZ width and dislocations on grain boundaries play an important role in the IGC resistance.

CRediT authorship contribution statement

Lan-ping HUANG: Conceptualization, Formal analysis, Writing − Review and editing; **Long-long HE:** Data curation, Formal analysis, Writing − Original draft, Investigation; **Song LI:** Conceptualization, Funding acquisition, Supervision, Writing − Review and editing; **Wen-sheng LIU:** Resources, Funding acquisition; **Jing HUANG:** Investigation; **Song-yi CHEN:** Investigation.

Declaration of competing interest

The authors declare that they have no known

competing financial interests or personal relationships that could have appeared to influence the work reported in this paper.

Acknowledgments

This work was primarily financially supported by the National Natural Science Foundation of China (No. 51871245), the National Key R&D Program of China (No. 2017YFE0301505), and State Key Laboratory for Powder Metallurgy as well as State Key Laboratory of Light Weight and High Strength Structural Materials, Central South University, China.

References

[1] WANG Ming, HUANG Lan-ping, LIU Wen-sheng, MA Yun-zhu, HUANG Bo-yun. Influence of cumulative strain on microstructure and mechanical properties of multi-directional forged 2A14 aluminum alloy [J]. Materials Science and Engineering A, 2016, 674: 40−51.

[2] ZHANG Yu-xun, YI You-ping, HUANG Shi-quan, DONG Fei, WANG Hui-min. Investigation of the quenching sensitivity of forged 2A14 aluminum alloy by time−temperature−tensile properties diagrams [J]. Journal of Alloys and Compounds, 2017, 728: 1239−1247.

[3] VARMA S K, SALAS D, CORRAL E, CHAWLA K K, MAHAPATRA R. Microstructural development during ageing of 2014 aluminum alloy composite [J]. Journal of Materials Science, 1999, 34: 1855−1863.

[4] CHEN Zai-liang, QIAN You-rong, XING Shu-yi, SUN Cheng-qing, ZHOU Jing-qi. Stress corrosion cracking behavior and two-step aging of high strength Al−Cu−Mg−Si alloy [J]. Journal of Chinese Society for Corrosion and Protection, 1988, 8(2): 135−140. (in Chinese)

[5] LI Peng-wei, LI Hui-zhong, LIANG Xiao-peng, HUANG Lan, ZHANG Ke-long, CHEN Zhi. Enhanced low-cycle fatigue and crack propagation resistance of an Al−Cu−Mg−Si forging alloy by non-isothermal aging [J]. Materials Science and Engineering A, 2018, 732: 341−349.

[6] FU Rong, HUANG Yuan-chun, LIU Yu, LI Hui, WANG Zhi-wen. Influence of homogenization treatment on microstructure and recrystallization behavior of 2195 Al−Li alloy [J]. Transactions of Nonferrous Metals Society of China, 2023, 33(8): 2255−2271.

[7] LIU L, CHEN J H, WANG S B, LIU C H, YANG S S, WU C L. The effect of Si on precipitation in Al−Cu−Mg alloy with a high Cu/Mg ratio [J]. Materials Science and Engineering A, 2014, 606: 187−195.

[8] LI Fu-shan, CHEN Song-yi, CHEN Kang-hua, HUANG Lan-ping. The role of Si on microstructure, mechanical and local corrosion behaviors of an Al−Cu−Mg−Si alloy with high Cu/Mg ratio [J]. Journal of Alloys and Compounds, 2020, 819: 152977-1-9.

[9] CHEN Zhi-guo, ZHANG Ji-shuai, SHU Jun, SHA Gang, XIA Jun-hai, WANG Shi-yong, RINGER S P. Effects of Si addition on the microstructure evolution of Al−Cu−Mg alloys in the α+S+T phase field [J]. Philosophical Magazine Letters, 2013, 93: 648−654.

[10] MARTIN J W. Precipitation hardening: Theory and applications [M]. Butterworth−Heinemann, 2012.

[11] WANG Cong, LUO Bing-hui, XIONG Wen-ying, WANG Zhi-chao. Effect of pre-stretching on microstructure and mechanical properties of 2024 aluminum alloy plate [J]. Light Alloy Fabrication Technology, 2011, 39(10): 63−68. (in Chinese)

[12] ZHANG Xin-ming, LIU Ling, JIA Yu-zhen. Effects of stretching and rolling pre-deformation on microstructures and mechanical properties of 2519A aluminum alloy [J]. The Chinese Journal of Nonferrous Metals, 2010, 20(6): 1088−1094. (in Chinese)

[13] QUAN Li-wei, ZHAO Gang, GAO Sam, MUDDLE B C. Effect of pre-stretching on microstructure of aged 2524 aluminium alloy [J]. Transactions of Nonferrous Metals Society of China, 2011, 21(9): 1957−1962.

[14] LU Ding-ding, LI Jin-feng, NING Hong, MA Peng-cheng, CHEN Yong-lai, ZHANG Xu-hu, ZHANG Kai, LI Jian-mei, ZHANG Rui-feng. Effects of microstructure on tensile properties of AA2050-T84 Al−Li alloy [J]. Transactions of Nonferrous Metals Society of China, 2021, 31(5): 1189−1204.

[15] LI Ji-yu, CHEN Song-yi, LI Fu-shan, CHEN Kang-hua, HUANG Lan-ping. Synergy effect of Si addition and pre-straining on microstructure and properties of Al−Cu−Mg alloys with a medium Cu/Mg ratio [J]. Materials Science and Engineering A, 2019, 767: 138429.

[16] LIU Xiao-yan, WANG Zhao-peng, LI Qing-shuai, ZHANG Xi-liang, CUI Hao-xuan, ZHANG Xiao-liang. Effects of pre-deformation on microstructure and properties of Al−Cu−Mg−Ag heat-resistant alloy [J]. Journal of Central South University, 2017, 24: 1027−1033. (in Chinese)

[17] LI Yao, LIU Zhi-yi, BAI Song, LIN Liang-hua, GAO Li-fang. Effects of pre-strain on exfoliation corrosion behavior in Al−Cu−Mg alloy [J]. Journal of Materials Engineering and Performance, 2012, 21: 1479−1484.

[18] LUO C, ZHOU X, THOMPSON G E, HUGHES A E. Observations of intergranular corrosion in AA2024-T351: The influence of grain stored energy [J]. Corrosion Science, 2012, 61: 35−44.

[19] LAN Jian, SHEN Xue-jun, LIU Juan, HUA Lin. Strengthening mechanisms of 2A14 aluminum alloy with cold deformation prior to artificial aging [J]. Materials Science and Engineering A, 2019, 745: 517−535.

[20] GHOSH S K. Influence of cold deformation on the aging behaviour of Al−Cu−Si−Mg alloy [J]. Journal of Materials Science & Technology, 2011, 27(3): 193−198.

[21] HUANG Lan-ping, HE Long-long, CHEN Song-yi, CHEN Kang-hua, LI Ji-yu, LI Song, LIU Wen-sheng. Effects of non-isothermal aging on microstructure, mechanical properties and corrosion resistance of 2A14 aluminum alloy [J]. Journal of Alloys and Compounds, 2020, 842: 155542-1-14.

[22] GB/T 7998—2005. Test method for inter-granular corrosion of aluminum alloys [S].

[23] BASSANI P, GARIBOLDI E, VIMERCATI G. Calorimetric analyses on aged Al−4.4Cu−0.5Mg−0.9Si−0.8Mn alloy (AA2014 grade) [J]. Journal of Thermal Analysis and Calorimetry, 2007, 87: 247−253.

[24] UNGÁR T. Dislocation densities, arrangements and character from X-ray diffraction experiments [J]. Materials Science and Engineering A, 2001, 309/310: 14−22.

[25] UNGÁR T, DRAGOMIR I, RÉVÉSZ A, BORBÉLY A. The contrast factors of dislocations in cubic crystals: The dislocation model of strain anisotropy in practice [J]. Journal of Applied Crystallography, 1999, 32: 992−1002.
[26] CHAKRABARTI D J, LAUGHLIN D E. Phase relations and precipitation in Al−Mg−Si alloys with Cu additions [J]. Progress in Materials Science, 2004, 49: 389−410.
[27] ESKIN D G. Decomposition of supersaturated solid solutions in Al−Cu−Mg−Si alloys [J]. Journal of Materials Science, 2003, 38: 279−290.
[28] DUAN Q Q, QU R T, ZHANG P, ZHANG Z J, ZHANG Z F. Intrinsic impact toughness of relatively high strength alloys [J]. Acta Materialia, 2018, 142: 226−235.
[29] WANG S C, STARINK M J. Two types of *S* phase precipitates in Al−Cu−Mg alloys [J]. Acta Materialia, 2007, 55: 933−941.
[30] RINGER S P, SOFYAN B T, PRASAD K S, QUAN G C. Precipitation reactions in Al−4.0Cu−0.3Mg (wt.%) alloy [J]. Acta Materialia, 2008, 56: 2147−2160.
[31] RIOTINO G, ZANAD A. Coupled formation of hardening particles on pre-precipitates in an Al−Cu−Mg−Si 2014 alloy [J]. Materials Letters, 1998, 37: 241−245.
[32] DUTTA I, HARPER C P, DUTTA G. Role of Al_2O_3 particulate reinforcements on precipitation in 2014 Al-matrix composites [J]. Metallurgical and Materials Transactions A, 1994, 25: 1591−1602.
[33] GAO X, NIE Jian-feng, MUDDLE Barry C. Effects of Si additions on the precipitation hardening response in Al−Cu−Mg(−Ag) alloys [J]. Materials Science Forum, 1996, 217−222: 1251−1256.
[34] RINGER S P, HONO K, POLMEAR I J, SAKURAI T. Nucleation of precipitates in aged Al−Cu−Mg−(Ag) alloys with high Cu:Mg ratios [J]. Acta Materialia, 1996, 44: 1883−1898.
[35] GABLE B M, ZHU A W, CSONTOS A A, STARKE E A. The role of plastic deformation on the competitive microstructural evolution and mechanical properties of a novel Al−Li−Cu−X alloy [J]. Journal of Light Metals, 2001, 1(1): 1−14.
[36] BISWAS A, SIEGEL D J, SEIDMAN D N. Compositional evolution of Q-phase precipitates in an aluminum alloy [J]. Acta Materialia, 2014, 75: 322−336.
[37] LI Hui-zhong, ZHU Ze-xiao, LIANG Xiao-peng, LI Peng-wei, QI Ye-long, LÜ Feng, HUANG Lan. Effect of T6-treatments on microstructure and mechanical properties of forged Al−4.4Cu−0.7Mg−0.6Si alloy [J]. Transactions of Nonferrous Metals Society of China, 2017, 27: 2539−2547.
[38] BIRBILIS N, BUCHHEIT R G. Electrochemical characteristics of intermetallic phases in aluminum alloys−An experimental survey and discussion [J]. Journal of the Electrochemical Society, 2005, 152(4): 140−151.
[39] SINHMAR S, DWIVEDI D K. A study on corrosion behavior of friction stir welded and tungsten inert gas welded AA2014 aluminium alloy [J]. Corrosion Science, 2018, 133: 25−35.
[40] GHOSH K S, DAS K, CHATTERJEE U K. Correlation of stress corrosion cracking behavior with electrical conductivity and open circuit potential in Al−Li−Cu−Mg−Zr alloys [J]. Materials and Corrosion, 2007, 58: 181−188.
[41] KARAYAN A I, JATA K, VELEZ M, CASTANEDA H. On exfoliation corrosion of alloy 2060 T8E30 in an aggressive acid environment [J]. Journal of Alloys and Compounds, 2016, 657: 546−558.
[42] ROBINSON M J. Mathematical modelling of exfoliation corrosion in high strength aluminium alloys [J]. Corrosion Science, 1982, 22: 775−790.
[43] MA Zhi-min, LIU Jia, YANG Zhen-shen, LIU Sheng-dan, ZHANG Y. Effect of cooling rate and grain structure on the exfoliation corrosion susceptibility of AA 7136 alloy [J]. Materials Characterization, 2020, 168: 110533.

预拉伸对 2A14 铝合金显微组织、力学性能和腐蚀性能的影响

黄兰萍[1,2]，何龙龙[1,3]，李 松[1,3]，刘文胜[1,2]，黄 静[1,3]，陈送义[4,5]

1. 中南大学 粉末冶金研究院，长沙 410083；
2. 中南大学 轻质高强结构材料国家级重点实验室，长沙 410083；
3. 中南大学 粉末冶金国家重点实验室，长沙 410083；
4. 中南大学 轻合金研究院，长沙 410083；
5. 中南大学 有色金属先进结构材料与制造协同创新中心，长沙 410083

摘 要：研究预拉伸变形量对峰值时效态 2A14 铝合金显微组织、力学性能和腐蚀行为的影响。结果表明：由于预拉伸导致细小弥散的 θ'相在基体中大量析出，合金的硬度和强度都明显提升；在峰值时效前引入预拉伸可以明显提高峰值时效硬度并加快到达峰值时效时间；当预拉伸变形量为 7.5%时，θ'相的分布明显变得更不均匀，这导致极限抗拉强度的下降；随着预拉伸变形量增加，合金塑性、冲击韧性和剥落腐蚀抗力均逐渐下降，但晶间腐蚀抗力先提高后下降。

关键词：2A14 铝合金；预拉伸；显微组织；力学性能；腐蚀抗力

(Edited by Bing YANG)